Available online at www.sciencedirect.com
SCIENCE DIRECT®
Microelectronic Engineering 83 (2006) 1786–1791
MICROELECTRONIC ENGINEERING
www.elsevier.com/locate/mee

Nanofabrication of negative refractive index metasurfaces

Zoran Jakšić [a,*], Dana Vasiljević-Radović [a], Milan Maksimović [a], Milija Sarajlić [a], Aleksandar Vujanić [b], Zoran Djurić [a]

[a] *IHTM – Institute of Microelectronic Technologies and Single Crystals, Njegoseva 12, Belgrade 11000, Serbia and Montenegro*
[b] *IMA – Integrated Microsystems Austria, Viktor Kaplan Straße 2, 2700 Wiener Neustadt, Austria*

Available online 23 February 2006

Abstract

We designed and fabricated planar metamaterial 'particles' (metasurfaces) intended to achieve negative effective refractive index in mid-infrared. We considered double split ring resonators (negative permeability particles) with additional capacitive gaps to compensate for the inertial inductance, as well as complementary double split rings (negative permittivity). We calculated dispersion relations and considered scaling conditions for our structures. For the fabrication of our experimental samples we used scanning probe nanolithography with *z*-scanner movement in 20 nm thin silver layers sputtered on positive photoresist or on polycarbonate. The morphology of our structures was characterized by atomic force microscope. We utilized a line width of 80–120 nm and the nanolithographic groove depth in different samples ranged from 4 to 80 nm. We believe our approach could be useful as a simple and low-cost tool for fabrication, assessment and optimization of different metamaterial geometries before larger arrays of particles are fabricated using other, more sophisticated and complex methods.
© 2006 Elsevier B.V. All rights reserved.

Keywords: Nanolithography; Nanophotonics; Metamaterials; Mesoscopic optics; Subwavelength optics

1. Introduction

Metamaterials with negative refractive index (NRM – negative refractive index materials) [1–6] are an important new class of structures in modern electromagnetics, photonics, micro- and nanoengineering. These are artificial composite metallodielectric subwavelength structures designed to reach negative values of effective dielectric permittivity and magnetic permeability – and thus a negative refractive index – in a given frequency range.

There are many different phenomena peculiar for NRM – reversal of Snell's law, as well as that of the Doppler shift and of the Eerenkov effect [6], to mention only a few. The direction of the Poynting vector in a negative index metamaterial is opposite to that of the wavevector, i.e. the vectors of the electric and magnetic field and the wavevector form a left-oriented set, which is the reason why NRM are sometimes called left-handed materials.

The peculiar properties of NRM drew a great deal of attention in scientific circles and in 2003 these structures were ranked among the first scientific breakthroughs of the year [7]. A plethora of novel applications of NRM was proposed (e.g. nanometer sized-circuits for optical frequencies [8], subwavelength-sized resonant cavities [9], emittance and absorptance tailoring [10] and many others). For the micro- and nanoengineering community probably the most attractive application appears to be the possibility to fabricate the "perfect lenses" or the "superlenses", devices able to focus all Fourier components of a 2D image, including evanescent modes, and thus applicable for nanolithography with subwavelength resolutions, i.e. beyond the diffraction limit [11]. After initial controversies over that issue, the first experiments have proven the applicability of the concept [12,13].

Most of good metals have negative permittivity in ultraviolet range. The first proposed and still the most commonly used experimental building blocks with negative permeability are split ring resonators (SRR, also referred to in literature as 'particles' or 'meta-atoms') [6]. The SRRs

* Corresponding author. Tel.: +381 64 3257 897; fax: +381 11 182 995.
E-mail address: jaksa@nanosys.ihtm.bg.ac.yu (Z. Jakšić).

0167-9317/$ - see front matter © 2006 Elsevier B.V. All rights reserved.
doi:10.1016/j.mee.2006.01.197

are arranged in unit cells whose multiplication furnishes macroscopic NRM medium. Their negative permittivity counterpart which can be designed for any frequency range are complementary split ring resonators (CSRR) [14,15].

The optical range is surely the most interesting for the application of NRM in super-resolution lithography, however the nanofabrication of structures for this range is connected with formidable problems. One of them is the appearance of inertial inductance at small particle dimensions as a consequence of the ballistic transport through the SRR. Another one is the behavior of materials, mostly the frequency dispersion of metals and the appearance of strong damping at shorter wavelengths. Many experiments with the fabrication of NRM particles for the optical range are being currently done [16–18], but practically applicable NRMs at shorter optical frequencies remain yet to be implemented.

In this paper we analyze fabrication of the planar NRM ('metasurfaces') for the mid infrared range using scanning probe nanolithography. We analyzed different planar designs utilizing the split ring and complementary split ring structures and performed experiments on their fabrication using our scanning probe nanolithographic system. The fabricated samples were characterized by the atomic force microscopy (AFM).

2. Theory

The basic building block of NRM, the double split ring resonator (SRR), is a highly conductive structure in which the capacitance between its two rings is large and balances its inductance. The essential operating principle of SRR originates in its complex electromagnetic resonant capacitive and inductive response described by its equivalent L-C resonant circuit structure [19]. A time-varying magnetic field applied perpendicular to the rings surface induces currents which, in dependence on the electromagnetic resonant properties of the structure, produce a magnetic field that may either oppose or enhance the incident field, thus resulting in positive or negative effective permeability. Complementary split ring (CSRR) is a complementary geometry to that of an SRR and according to the Babinet principle it is a unit cell furnishing negative ε [14,15,20].

For a double SRR (Fig. 1) with rings of negligible thickness one may apply the Lorentz expression [16] for effective permeability

$$\mu_{\rm eff} = \mu_0\left(1 + \frac{\omega_{\rm p}^2}{\omega_0^2 - {\rm i}\Gamma\omega - \omega^2}\right) \quad (1)$$

where ω_0 is the resonant frequency (for which $\mu_{\rm eff} \to \pm\infty$), $\omega_{\rm p}$ is the plasma frequency (for which $\mu_{\rm eff} \to 0$) and Γ denotes losses.

According to Pendry et al. [3] the resonant frequency is approximately

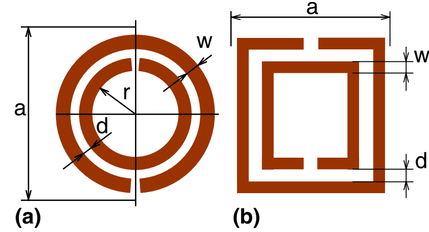

Fig. 1. Planar geometries of negative permeability material unit cells based on the split ring resonator: (a) circular structure; (b) square structure. Dark: thin metal film.

$$\omega_{0m} = \sqrt{\frac{3dc^2}{\pi^2 r^3}} \quad (2)$$

while the plasma frequency is

$$\omega_{\rm p} = \sqrt{\frac{3dc^2}{\pi^2 r^3 (1 - \pi r^2/a^2)}} \quad (3)$$

where a is the unit cell length, d is the gap between the rings, r is the inner split ring radius (see Fig. 1), while c is the speed of light in the medium when $\omega \to \infty$.

According to the Babinet principle, a CSRR structure exhibits an approximately dual behavior to that of the corresponding SRR [14] and (1)–(3) are then valid if one replaces $\mu_{\rm eff}$ with $\varepsilon_{\rm eff}$ [14,15].

Based on (1)–(3) the necessary unit cell dimensions to reach the optical wavelength range are readily calculated. Some calculated results are shown in Fig. 2 for the case when the ratio of the unit cell to the SRR radius is 0.4. According to it, the unit cell dimensions must be several times smaller than the operating wavelength, depending on the chosen gap within the SRR. If nanolithographic lines of the order of 0.1 μm are used (which defines the minimum gap between rings), structures with minimum features 1.5–4 μm can be designed, thus the target wavelengths would be about 5–10 μm (mid-infrared).

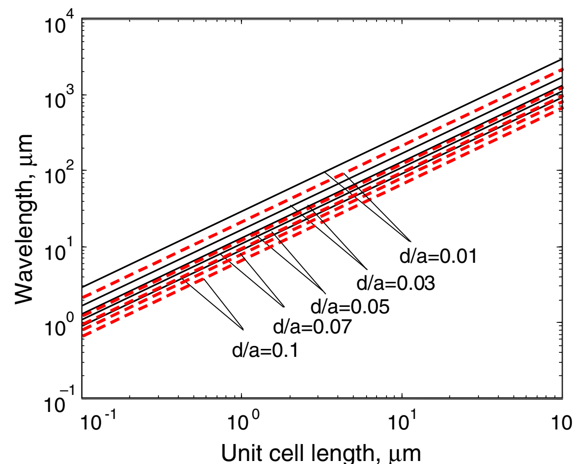

Fig. 2. Resonant wavelength (solid) and plasma wavelength (dashed) for double split ring resonators for different ratios of inter-ring gaps and unit cell lengths.

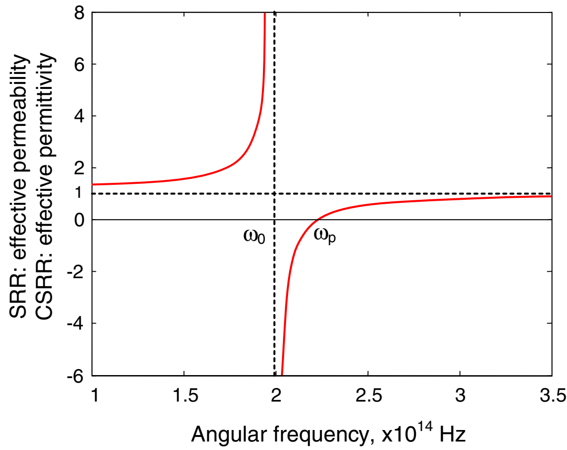

Fig. 3. Calculated frequency dependence of effective permeability for a split ring resonator. Identical dependence is valid for effective permittivity of a CSRR.

A calculated dispersion of effective magnetic permeability for a SRR (and, equivalently, dielectric permittivity for the corresponding CSRR) is shown in Fig. 3 for the case of low losses.

At optical frequencies the thickness of the metal layers should not be smaller than the skin depth [16] (approx. 20 nm for silver at 100 THz). Also, at these frequencies the inertial inductance appears, a consequence of the effective electron mass and the currents through the SRR becoming almost purely ballistic as wavelength decreases [6]. For the scaled-down dimensions the inertial inductance and damping effects prevail and the negative permeability/permittivity effect completely disappears. A method to improve performance of split rings at optical frequencies was proposed in [16] where additional capacitive gaps are introduced to the original SRR design.

Fig. 4 shows our modification of the above approach for the case of square and circular SRR and CSRR geometries. The top and bottom left drawings show split ring geometries with additional gaps, while the top and bottom right drawings correspond to the equivalent complementary split ring case. Curvilinear geometries are shown in the top row, and rectangular in the bottom row.

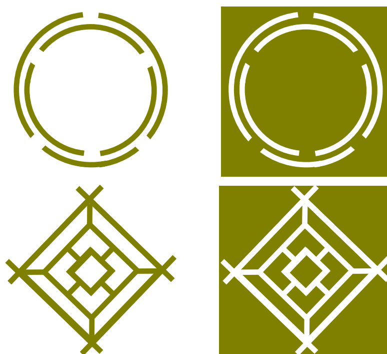

Fig. 4. Double split ring (left column) and complementary double split ring (right column), modified for high frequency operation by additional splits. Top row: curvilinear segments, bottom row: rectangular.

3. Experimental

We used polished silicon wafers as a substrate on which 400 nm thick positive photoresist was spin-coated and dried without baking. RF sputtering was utilized to deposit a 20 nm thick silver layer over the unbaked resist. Prior to nanolithography the surface morphology was characterized by atomic force microscopy (AFM). The achieved flatness was better than 2 nm. In our experiments we also used polycarbonate samples with a flatness of 10–30 nm.

The sample surfaces were nanolithographically processed to obtain NRM building blocks. To this purpose we utilized scanning probe nanolithography on our Veeco Autoprobe CP-Research atomic force microscope. Nanolithography was done under normal atmospheric pressure

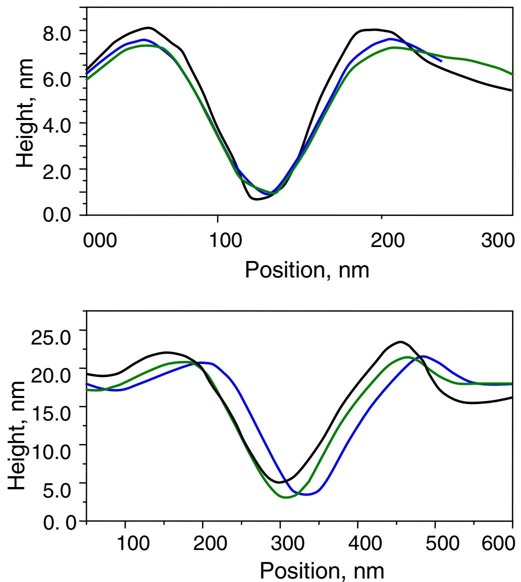

Fig. 5. Profiles of nanolithographic lines. Top: line profiles for silver on photoresist. Bottom: lines in polycarbonate substrate.

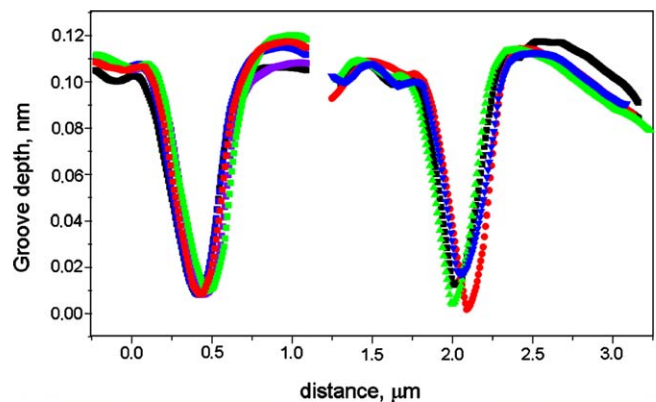

Fig. 6. Profilometry of 80–100 nm deep grooves in polycarbonate.

and at room temperature and humidity. No clean room conditions were necessary. Antivibration and shock-free conditions were ensured by an anti-vibration table unit with active oscillation dumping.

We utilized the *z*-scanner movement lithography ("scratching") with a silicon nitride microcantilever tip. The scanner base position was adjusted to between 0.7 and 0.9 μm below the zero position, thus pressing needle tip against the sample surface with forces of 50 nN.

Profilometry and morphology characterization of the obtained structures were done by AFM. A V-shaped cantilever was used, with a length 180 μm, thickness 25 μm and width 2 μm, stiffness 3.2 N/m, resonant frequency 95 kHz, tip shape sharpened pyramid, tip material Si_3N_4. Prior to characterization we performed standard calibration procedure of our system to ensure correct results. This was done by using test measurements on a set of standardized substrates with a given hardness. Characterization was done in microcantilever contact mode with a force of about 10 nN and was repeated for different magnifications and scanning speeds in order to obtain proper results.

Fig. 5 shows typical profiles of our nanolithographic lines.

It can be seen that the *z*-scanner movement nanolithography actually digs a furrow in the substrate, leaving upturned material on the edges. Another detrimental property of 'scratched' grooves is their very poor height-to-depth aspect ratio, as seen from the presented profiles. However, neither of these represents a problem in our case, since it was our intention only to physically disconnect thin metal surfaces while retaining the geometries shown in Fig. 4. Our nanolithographic lines were similar in width, depth to those described in [21] and were also done in similar materials. Larger depths have been obtained in polymeric surfaces, e.g., a few hundreds of nm in polymer surfaces [22] and even 50–60 nm in bulk metal [23] – both much larger than required for our structures. Generally,

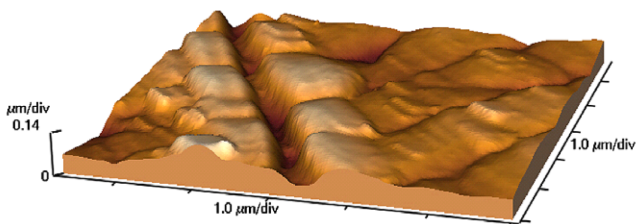

Fig. 7. Surface morphology of 80 nm deep line in polycarbonate.

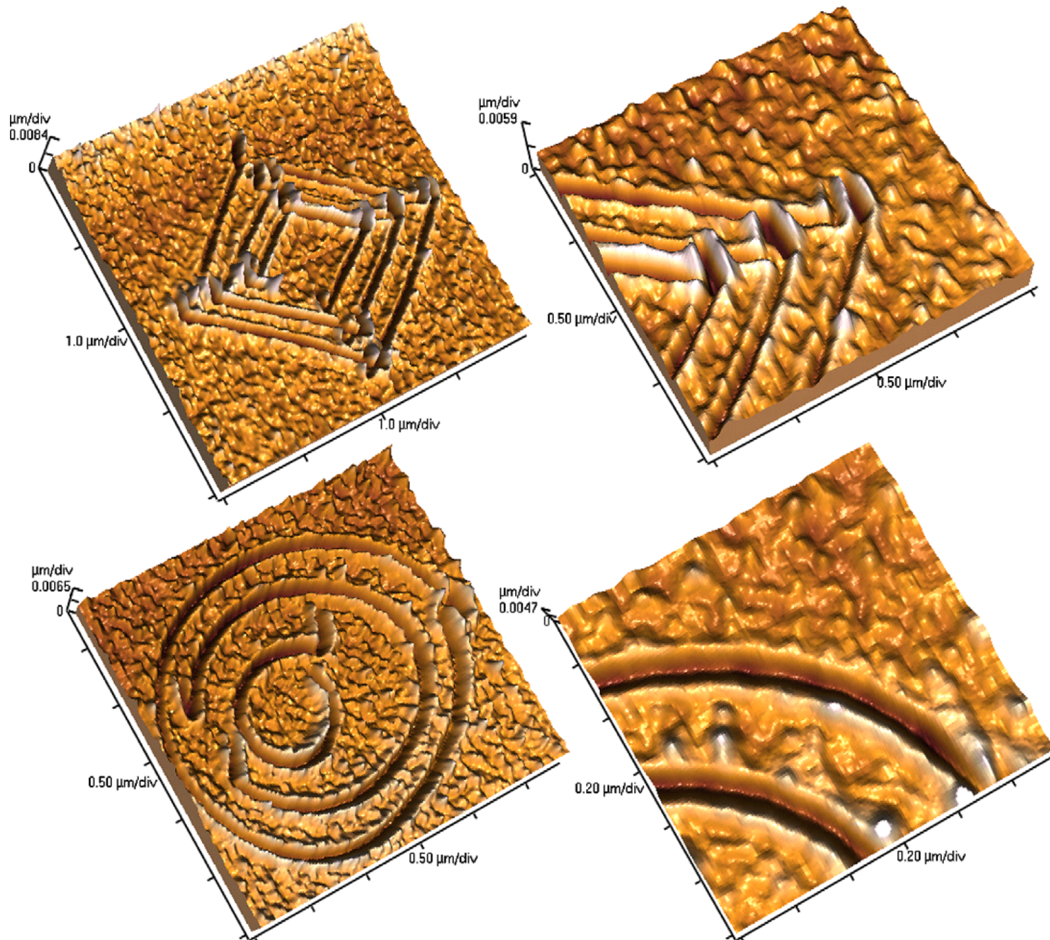

Fig. 8. Surface structures fabricated by *z*-scanner movement nanolithography in thin silver film on photoresist.

for many plasmonic structures (to which SRR and CSRR belong) it is often not important if the surface is broken or not, since already small corrugations enable surface plasmon operation and coupling with propagating modes.

Fig. 6 shows the results of AFM profilometric investigation for our samples with relatively larger groove depths (80 nm and deeper) fabricated in polycarbonate substrate, while Fig. 7 shows their surface morphology.

It can be again seen that the main problem with AFM lithography is its poor aspect ratio – the lithographic ‘‘scratches’’ are relatively wide and shallow. This means that due to the obtainable line width larger groove depths can be only used for structures for longer wavelengths – in the case shown in Figs. 6 and 7 these are at least 20 μm or more.

Fig. 8 shows our fabricated structures fabricated in thin silver layer on unbaked photoresist. The top row shows the rectangular features, and the bottom row curvilinear ones. The complete patterns are given on the left (top and bottom), while magnified details of each are shown on the right. In all cases the structures were about 2 μm wide, while its innermost dimension was about 1 μm. The *z*-scanner displacement was −0.7 μm and the nanolithographic line width was 80–120 nm. The position of some lines in the obtained structure deviated 60–150 nm from the designed location. Repeatability was tested by nanofabricating several identical pattern and it also ranged between 60 and 150 nm.

The process duration for a single SRR or CSRR took several seconds for straight-line segments, but it lasted 2–3 min for each curvilinear feature. Additionally, each nanolithographic pattern required full surface scanning before and after the process. Thus the fabrication of more complex patterns containing a large number of elements (‘particles’) could be painstakingly slow and the method remains convenient for simpler structures and small numbers of particles.

Among the largest problems noted with the nanofabrication of the SRR and CSRR geometries was deviation of the fabricated patterns compared to the designed ones, most noticeable in slight curving of otherwise straight segments or in designed circles becoming spirals. An additional problem was that in some patterns a ‘kink’ appeared at the beginning and at the end of each line, 100–300 nm long, probably caused by the operation of the piezo-actuated micropositioner.

An advantageous property of the sputter-deposited thin silver layers (in contrast to bulk metal) was that these were readily patterned by the silicon nitride needle tip (contrary to bulk metal).

4. Conclusion

In our experiments we used the well-known and relatively simple method of scanning-probe nanolithography to produce modified SRR and CSRR unit cells for the NRM in optical wavelength range. We fabricated our structures by the *z*-scanner movement SPM nanolithography in 20 nm thick silver layers and characterized them by AFM. The groove depth in different samples ranged from 4 to 80 nm. The utilized line width was 80–120 nm, and the repeatability 60–150 nm, depending on the process conditions and the feature complexity. We showed that it was possible to obtain required metasurface geometries in unbaked resist and polycarbonate substrates in spite of poor aspect ratio obtained by scanning probe lithography.

Our next efforts will be dedicated to electromagnetic characterization, and especially to magnetic force microscopy of metasurfaces. Later on, we also intend to combine SRRs and CSRRs into functional NRM structures and to measure their spectral transmission by IR microscopy. To do so, it will be necessary to choose among the fabricated prototyped structures and, once these are combined, to fabricate much larger arrays using, e.g., ion beam lithography.

We believe our approach could be useful when producing single and unique experimental structures because it simplifies the procedures, lowers the costs and reduces the necessary process duration. It does not compete with modern lithography methods which are still unavoidable for production of macroscopically large arrays of metamaterial particles, but we do believe it could be used as a simple and low-cost tool for the assessment of various metamaterial geometries before larger arrays of metaparticles are fabricated using other, more sophisticated and complex methods.

Acknowledgments

The authors thank Ms. Mirjana Popović, BSCE and Ms. Kristina Blagojević, IHTM-IMTM for their preparation of sample substrates. This work was partially funded by the Serbian Ministry of Science and Environmental Protection within the Project TR-6151B.

References

[1] V.G. Veselago, Sov. Phys. Uspekhi 10 (1968) 509.
[2] J.B. Pendry, A.J. Holdenz, D.J. Robbins, W.J. Stewartz, J. Phys. Condens. Matt. 10 (1998) 4785.
[3] J.B. Pendry, A.J. Holden, D.J. Robbins, W.J. Stewart, IEEE Trans. Microw. Theory Tech. 47 (1999) 2075.
[4] D.R. Smith, W.J. Padilla, D.C. Vier, D.C. Nemal-Nasser, S. Schultz, Phys. Rev. Lett. 84 (2000) 4184.
[5] R.A. Shelby, D.R. Smith, S. Schultz, Science 292 (2001) 77.
[6] S.A. Ramakrishna, Rep. Prog. Phys. 68 (2005) 449.
[7] Editorial, Science 302 (2003) 2039.
[8] N. Engheta, A. Salandrino, A. Alù, Phys. Rev. Lett. 95 (2005) 095504.
[9] N. Engheta, IEEE Antenn. Wireless Propag. Lett. 1 (2002) 10.
[10] M. Maksimović, Z. Jakšić, Phys. Lett. A 342 (5–6) (2005) 497.
[11] J.B. Pendry, Phys. Rev. Lett. 85 (2000) 3966.
[12] D.O.S. Melville, R.J. Blaikie, C.R. Wolf, Appl. Phys. Lett. 84 (2004) 4403.
[13] N. Fang, H. Lee, C. Sun, X. Zhang, Science 308 (2005) 534.
[14] F. Falcone, T. Lopetegi, M.A.G. Laso, J.D. Baena, J. Bonache, M. Beruete, R. Marques, F. Martin, M. Sorolla, Phys. Rev. Lett. 93 (19) (2004) 197401-1.

[15] R. Marqués, J.D. Baena, M. Beruete, F. Falcone, T. Lopetegi, M. Sorolla, F. Martín, J. Garcia, J. Opt. A: Pure Appl. Opt. 7 (2005) S38.
[16] R.W. Ziolkowski, E. Heyman, Phys. Rev. E 64 (2001) 056625.
[17] S. O'Brien, D. McPeake, S.A. Ramakrishna, J.B. Pendry, Phys. Rev. B. 69 (2004) 241101-1.
[18] S. Linden, C. Enkrich, M. Wegener, Ji. Zhou, T. Koschny, C.M. Soukoulis, Science 306 (2004) 1351.
[19] S. Zhang, W. Fan, N.C. Panoiu, K.J. Malloy, R.M. Osgood, S.R.J. Brueck, Postdeadline Paper at OSA Topical Meeting on NanoPhotonics for Information Systems, April 15, 2005. Available from: <http://arxiv.org/ftp/physics/papers/0504/0504208.pdf>.
[20] J.D. Baena, J. Bonache, F. Martín, R. Marqués Sillero, F. Falcone, T. Lopetegi, M.A.G. Laso, J. García–García, I. Gil, M.F. Portillo, M. Sorolla, IEEE Trans. Microw. Theory Tech. 53 (2005) 1451.
[21] T.-H. Fang, C.-I. Weng, J.-G. Chang, Nanotechnology 11 (2000) 181.
[22] M.R. VanLandingham, L.P. Sung, N.K. Chang, T.Y. Wu, S.H. Chang, V.D. Jardret, JCT Res. 1 (2004) 257.
[23] D. Devecchio, P. Schmutz, G.S. Frankel, Electrochem. Solid-State. Lett. 3 (2000) 90.